Self-luminescent PVDF membrane hybrid with rare earth nanoparticles for real-time fouling indication

Kai Fan [a,b], Jianxi Huang [b], Enmei Liu [a], Jun Hu [b,c], Haijun Yang [b,c,*]

[a] School of Architecture and Materials, Chongqing College of Electronic Engineering, Chongqing, 401331, China
[b] Division of Interfacial Water, CAS Key Laboratory of Interfacial Physics and Technology, Shanghai Institute of Applied Physics, Chinese Academy of Sciences, Shanghai, 201800, China
[c] Shanghai Synchrotron Radiation Facility, Zhangjiang Laboratory (SSRF, ZJLab), Shanghai Advanced Research Institute, Chinese Academy of Sciences, Shanghai, 201204, China

ARTICLE INFO

ABSTRACT

A kind of hybrid membrane with self-luminescent property was prepared by mixing rare earth nanoparticles of nano-$Sr_4Al_2O_4$: Eu^{2+}, Dy^{3+} into the casting solution dissolved with polyvinylidene fluoride (PVDF), and then coprecipitated through non-solvent induced phase separation (NIPS) method. Membrane were characterized by luminescent intensity, scanning electron microscopy (SEM), atomic force microscopy (AFM), contact angle measurement, and the results showed that the membranes with the nano-$Sr_4Al_2O_4$: Eu^{2+}, Dy^{3+} content of 0.75 wt % have the highest luminescent intensity and the lowest contact angle, but further increasing the nanoparticle content will decrease the surface pore density and change the cross-sectional structure. Meanwhile, the membrane permeability and the rejection rate proved that the addition of nano-$Sr_4Al_2O_4$: Eu^{2+}, Dy^{3+} effectively improved the flux of water and Bovine Serum Albumin/Humic Acid (BSA/HA) aqueous solution through the membrane. This hybrid membrane possessed the performance of real-time response to membrane pollution/ cleaning, and finally an effectively improvement of anti-pollution property.

1. Introduction

Membrane filtration process has been extensively used in many industries, such as the mean water recycling in construction, industrial waste water treatment, purification of drinking water etc., mainly due to its high efficiency, selectivity and non-secondary pollution [1]. However, the adsorption of nonpolar solutes, hydrophobic particles or bacteria onto/into its surface/pores always causes severer fouling problem, resulting in a higher energy demand, shorter membrane lifetime, and unpredictable separation performance [2–4].

To restore membrane's separation performance, periodic cleaning processes were usually designed based on the attenuation of the flux and pressure change during the filtration operation [5]. The change of reduced transmembrane pressure (TMP) was currently most commonly used to define the degree of membrane fouling and washing efficiency [6]. G. Sun et al. used the change of TMP to reflect the membrane pollution [7]. Bo Hu et al. realized the characterization of membrane fouling through a standard transmembrane pressure step method based on TMP variation [8]. However, membrane-fouling evaluation based on TMP variation can only explain the performance of the whole membrane components, but not accurately reflected the details, especially for the case of multi-component series connection [9]. Thus, an indicator that can real time evaluate membrane's pollution/cleaning level is critical to further improve the separation efficiency and the performance of membrane.

Rare earth up conversion luminescent nanoparticles, which have abundant electronic energy levels and 4f electronic orbit in the atom of rare earth elements, can create multiple energy level transitions [10]. It can adsorb or emit light with the wavelength from ultraviolet to infrared regions, obtaining various luminescent properties [11]. Generally, the illumination lux is linearly proportional to the incident light intensity [12,13]. Thus, it should be a good candidate as a pollution indicator in a hybrid membrane where pollutants always block a part of the incident light. Moreover, because rare earth self-luminescent nanoparticles contain a large amount of metal salts, the addition of which in polymer membranes should significantly improve the permeation and

---

Table 1
Quantity of materials used for synthesis of membrane.

| Membrane ID	PVDF/ g	$Sr_4Al_2O_4$: Eu^{2+}, Dy^{3+}/ g	NMP/ g	PVP/ g	Total/ g
1	15	0	81	4	100
2	15	0.25	80.75	4	100
3	15	0.5	80.5	4	100
4	15	0.75	80.25	4	100
5	15	1.00	80	4	100

Table 2
Static contact angle measurements.

Fraction of $Sr_4Al_2O_4$: Eu^{2+}, Dy^{3+} (wt.%)	Contact angle (deg)	Standard deviation (SD)
0	89.9	3.62
0.25	86.7	5.18
0.50	82.4	5.26
0.75	78.1	4.70
1.00	78.0	5.33

anti-fouling performance of the prepared hybrid membranes, similar to other inorganic nanoparticles such as Al_2O_3 [14–16], TiO_2 [17–19], ZnO [20] and ZrO_2 [21,22] etc.

Here, we introduced nano-$Sr_4Al_2O_4$: Eu^{2+}, Dy^{3+} into the casting solution of PVDF filtration membrane to prepare a self-luminescent membrane, where $Sr_4Al_2O_4$ was the luminescent "substrate", Eu^{2+} and Dy^{3+} the "activator". Different mass fraction of rare earth nanoparticles was employed to systematically examine their impact on membrane luminescent intensity, then membrane characteristics were comprehensively investigated by SEM for the pore size, pore distribution, porosity and element distribution of synthesized membranes, AFM for mapping the topography and the surface roughness, and contact angle for hydrophilicity of membrane surface. In addition, the water flux of different membranes was tested by using the membrane evaluation system platform. Through the practice of the aqueous solution dissolved with BSA and humic acid, the effect of this hybrid membranes' real time responding to membrane pollution was discussed. Finally, we also assessed the effect of the addition of rare earth nanoparticles on the anti-fouling performance of the membranes.
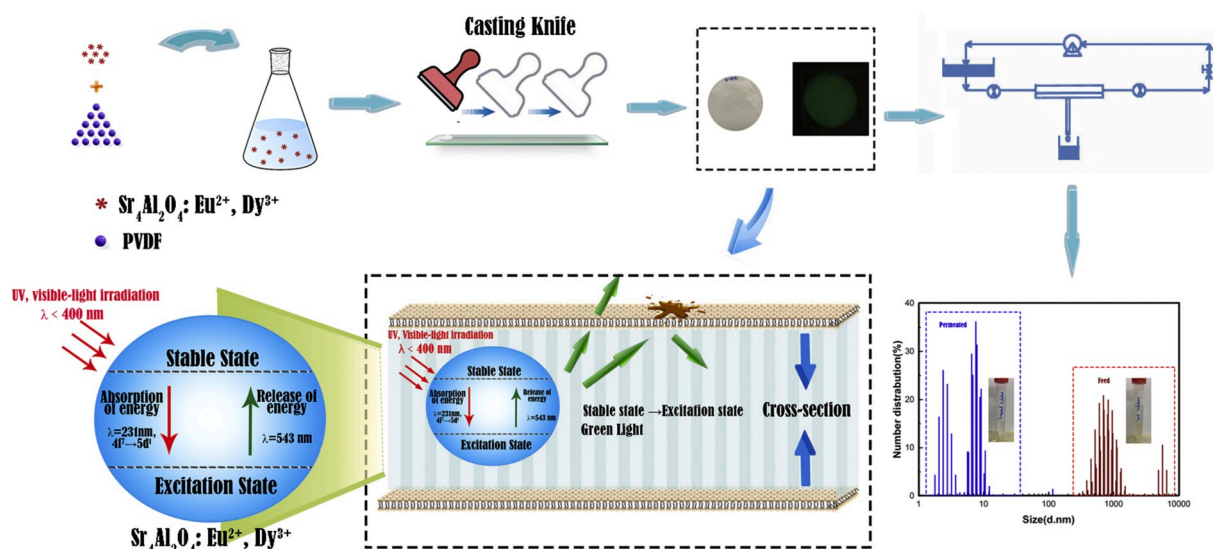
Scheme 1. Schematic illustration of the preparation of self-luminescent hybrid membrane and its luminescence mechanism.

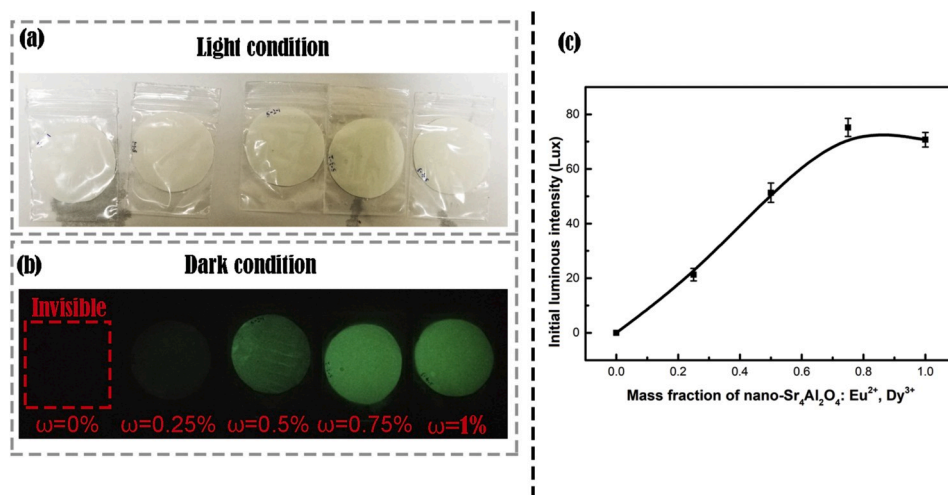**Fig. 1.** The luminescent performance of pristine PVDF membrane and hybrid membranes with different nano-$Sr_4Al_2O_4$: Eu^{2+}, Dy^{3+} mass fractions under light (a) and dark (b) conditions, and (c) the curve of luminescent intensity change with mass fraction.
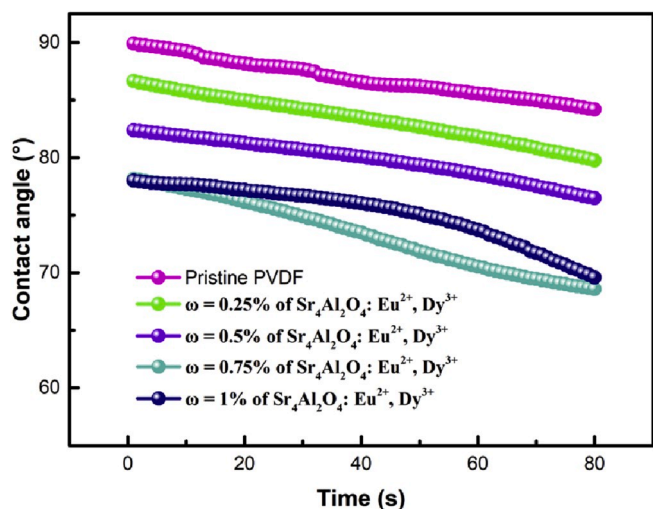
Fig. 2. Membrane contact angles change with time.

2. Experimental

2.1. Materials

Poly(vinylidene fluoride) (PVDF, in powder form) was purchased from Solvay Chemicals Company, Belgium. N-methyl pyrrolidone (NMP), polyethylene glycols (PEG), Bovine Serum Albumin (BSA) and humic acid (HA) were purchased from Sinopharm Chemical Reagent Co., Ltd. Nano-$Sr_4Al_2O_4$: Eu^{2+}, Dy^{3+} in powder form passed by 200 mesh screening was purchased from Chongqing Zero-one Environmental Technology Co., Ltd. Water purified with a Milli-Q system from Millipore was used for all experiments. PVDF should be rinsed with 40 °C deionized water to remove impurities and then dried in vacuum condition at 70 °C till a constant weight has been reached before using. All organic solvents were analytical reagent (AR), and other materials mentioned above were used without further purification.

2.2. Membranes preparation

Membranes were prepared by using Non-solvent Induced Phase Separation (NIPS) method under the following procedure:

As showed in Scheme 1, pristine PVDF and nano-$Sr_4Al_2O_4$: Eu^{2+}, Dy^{3+} powder, PVP and NMP solvent were mixed together within a certain proportion shown in Table 1. The mixtures were stirred at 60 °C for 3 days and then rested at room temperature for 2 days, (showed in Fig. S1 of supporting information). After that, solutions were cast onto a glass plate by using a 0.2 mm thick cast knife and the obtained solutions were immersed in a water bath of 19 °C with the glass plate for several minutes until the formation of membranes and their separation from the glass plate. The formed membranes were kept in fresh deionized water changing every 6 h for further characterization. It should be pointed out that the heating process, the stirring rate and the viscosity of the casting solution should be carefully controlled during the membrane preparation process to prevent the hybrid nanoparticles from agglomeration which will negatively affect the structure and performance of the prepared hybrid membranes.

2.3. Membrane luminescent intensity

Membrane's luminescent intensity could be tested by a high resolution illuminometer (ST-80C), which was purchased from Shenzhen Huashengchang Technology Industry Co., Ltd. All membranes were firstly placed under full illumination light condition for 10 min, then the light source was removed and the luminescent intensity of the

membranes was tested.

2.4. Contact angle measurements

Contact angle measurements of membranes were performed on an Attension Theta System (KSV Instruments Ltd., Finland). About 5μL water drop was lowered onto the membrane surface with a needle tip. Then, a magnified image of the droplet was recognized by a digital camera. All contact angles were determined from these images with the built-in calculation software.

2.5. Morphology study

Scanning electron microscope (SEM) images of surface and cross-section of membranes was carried out on a LEO1530vp SEM (Germany), at a voltage of 10 kV and the current of 10 mA. To obtain cross-section images at different magnifications, membranes were immersed in liquid nitrogen and fractured. These samples were then attached on a carbon tape and sputtered with gold. During the membrane surface morphology analysis, the average pore diameter ($D_{average}$), pore density, surface porosity (ε) were obtained and calculated by software analysis (Image-Pro Plus 6.0). Meanwhile, C, Al and Eu elements on the membrane surface and cross-section were simultaneously analyzed by energy dispersive X-ray spectroscopy (EDX).

2.6. Atomic force microscopy (AFM) analysis

Membrane surface roughness was measured by using Multimode 8 SPM AFM (Bruker, Germany) instrument, with an AFM tip of DNP-10 product by Bruker company. Membrane samples were fixed on a specimen holder, and 10 μm × 10 μm areas were scanned in the acoustic alternating current (AC) tapping mode. At least five replicates were performed for each membrane sample. All image data were analyzed and processed with offline analysis software "nanoscope analysis" provided by the Bruker device.

2.7. Membrane permeability, rejection and anti-fouling tests

All membrane permeability, rejection and anti-fouling property tests were conducted by the Convergence Inspector-Poseidon testing platform, (see Fig. S2 in supporting information for more details). The effective membrane area was 35.3 cm^2. The feed flux of membrane was set at 2 kg/h and the operating pressure was configured at 0.5 bar. The membrane water flux was measured by feeding solution with deionized water, while the BSA/HA aqueous solution flux of the membrane was replaced to an aqueous medium solution with 0.15 g/L of humic acid and 0.15 g/L of BSA. The membrane rejection was calculated by Eq. (1):

$$R = 1 - \frac{C_p}{C_f} \times 100\% \tag{1}$$

where, C_p and C_f are the concentrations of the probe solute in permeate and feed, respectively and were determined from the total organic carbon measured by using a TOC analyzer (Shimadzu TOC-5000A).

Meanwhile, the particle size of the feed solution and permeated solution were measured by using the Delsa NanoC particles Analyzer (BECKMAN COULTER, American), The mean/hydrodynamic diameter was determined via a cumulative analysis.

The anti-fouling experiment of the membrane was carried out on the same test platform by the following set procedure: firstly, deionized water pressure through membrane was introduced for 40 min to remove bubbles, and then the BSA/HA aqueous solution with same concentration mentioned before was introduced. When this aqueous solution flux decreased to 20% of the initial, the forward flushing and back flushing were carried out. The above steps were repeated for 6 to 7 times to fully verify the anti-fouling performance of the membrane.
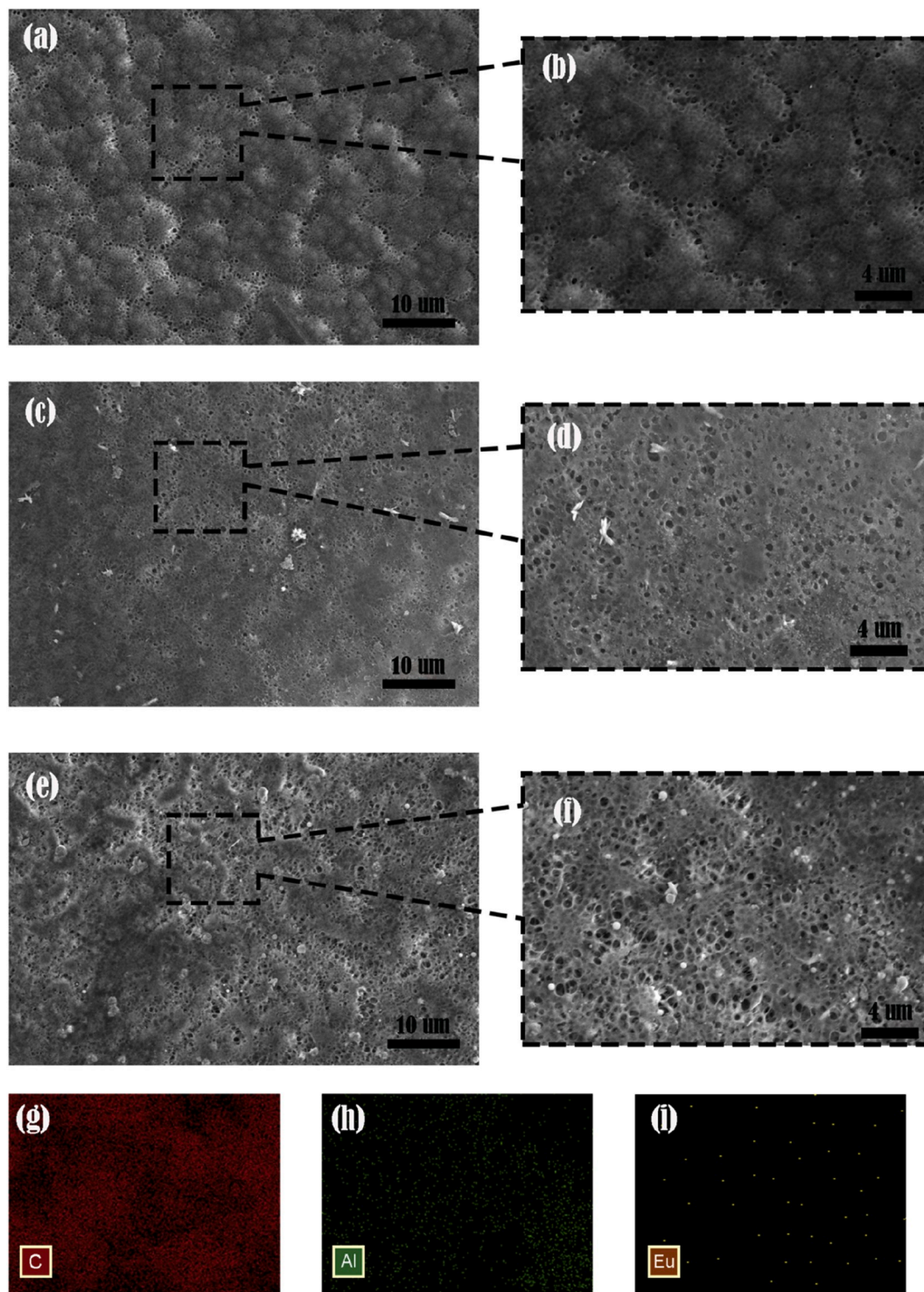
Fig. 3. SEM images of membrane top surfaces: (a) and (b) magnification of pristine PVDF membrane, (c) and (d) magnification of hybrid membrane with 0.50 wt% of nano-$Sr_4Al_2O_4$: Eu^{2+}, Dy^{3+}, (e) and (f) magnification of hybrid membrane with 1.00 wt% of nano-$Sr_4Al_2O_4$: Eu^{2+}, Dy^{3+}, EDX mapping images of (g–i) hybrid membrane with 0.50 wt% of nano-$Sr_4Al_2O_4$: Eu^{2+}, Dy^{3+}.

Table 3
Summary of pore size distribution statistics.

Fraction of $Sr_4Al_2O_4$: Eu^{2+}, Dy^{3+} (wt. %)	$D_{average}$ (nm)	Pore density (m^{-2})	ε (%)
0	17 ± 4	5.23×10^{13}	3.78
0.25	23 ± 7	4.68×10^{13}	9.45
0.50	15 ± 3	2.38×10^{13}	5.66
0.75	31 ± 7	2.15×10^{13}	6.21
1.00	22 ± 6	1.01×10^{13}	3.50

Table 4
The surface elemental compositions of different membranes.

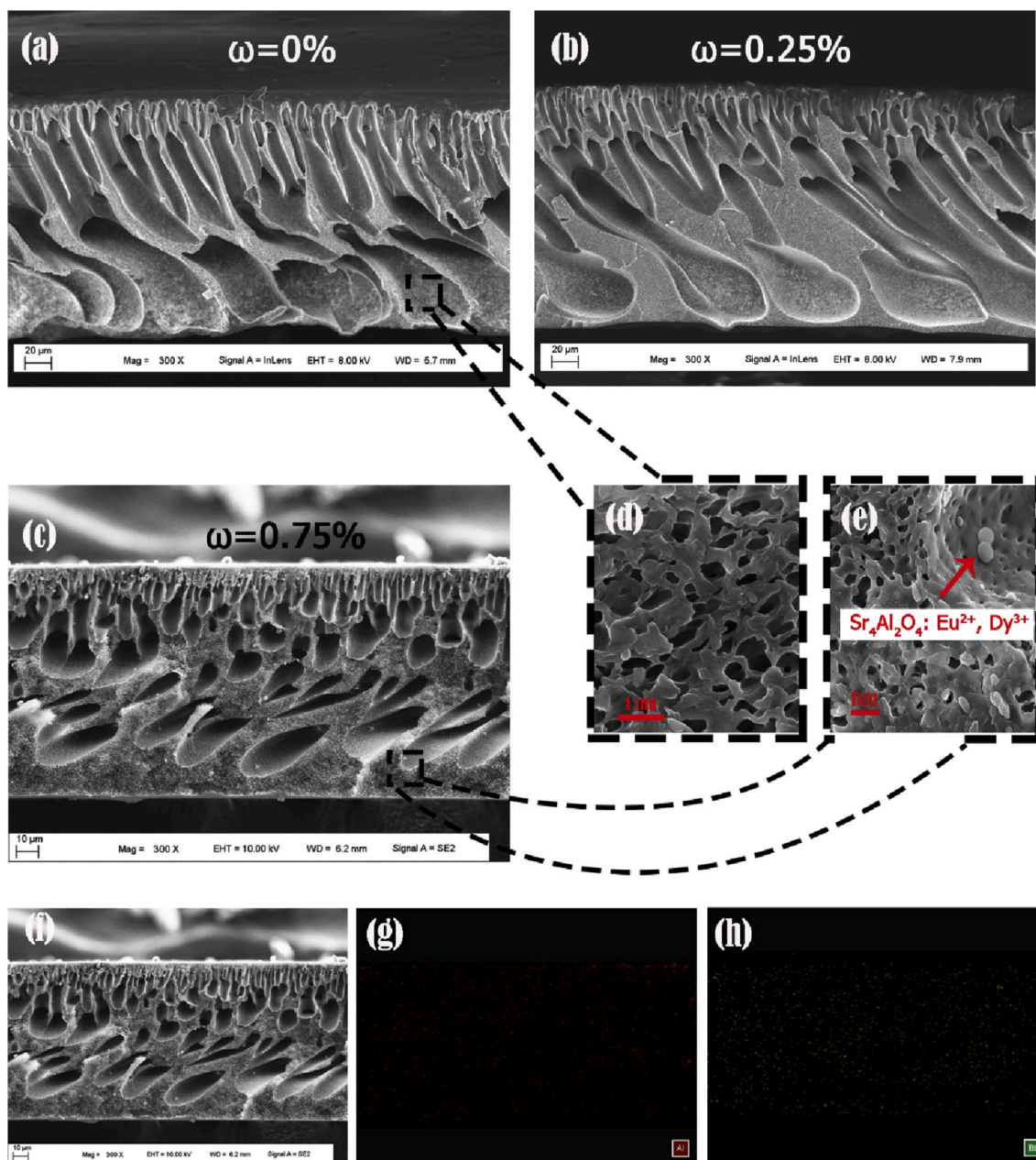| Fraction of $Sr_4Al_2O_4$: Eu^{2+}, Dy^{3+} (wt.%)	C (%)	Al (%)	Eu (%)
0	54.83	0	0
0.25	55.46	0.37	0.01
0.50	57.49	0.68	0.04
0.75	54.02	1.35	0.08
1.00	56.17	0.87	0.06

Fig. 4. SEM images of membrane cross sections: (a) pristine PVDF membrane, (b) hybrid membrane with 0.25 wt% of nano-$Sr_4Al_2O_4$: Eu^{2+}, Dy^{3+}, (c) hybrid membrane with 0.75 wt% of nano-$Sr_4Al_2O_4$: Eu^{2+}, Dy^{3+}, amplification of (d) pristine PVDF membrane and (e) hybrid membrane with 0.75 wt% of nano-$Sr_4Al_2O_4$: Eu^{2+}, Dy^{3+}, EDX mapping images of (f–h) hybrid membrane with 0.75 wt% of nano-$Sr_4Al_2O_4$: Eu^{2+}, Dy^{3+}.

3. Results and discussion

3.1. Luminescent intensity of membranes

The self-luminescence of the hybrid membrane is affected by the properties, amount and distribution of rare earth nanoparticles added to the membrane. Fig. 1 shows the luminescent performance of pristine PVDF membrane and hybrid membranes with different nano-$Sr_4Al_2O_4$: Eu^{2+}, Dy^{3+} mass fractions under light and dark conditions. Under the light condition, the hybrid membranes with rare earth nanoparticles were not obviously different from the original PVDF membrane. However, in the dark condition, hybrid membranes displayed obvious luminescent properties, and the luminescent intensity increased with the addition of rare earth nanoparticles as showed in Fig. 1(a) and (b). Furthermore, the luminescent intensity of hybrid membranes was

measured by illumination photometer, and the results illustrate that the luminescent intensity of the hybrid membrane increase with the adding amount of rare earth nanoparticles within a certain range of added amount. When the amount of nano-$Sr_4Al_2O_4$: Eu^{2+}, Dy^{3+} reached to about 0.75 wt%, the luminescent intensity of the membrane reached its maximum (73.3 Lux). Further increases the mass fraction of rare earth

Table 5
The partial cross section elemental compositions of different membranes.

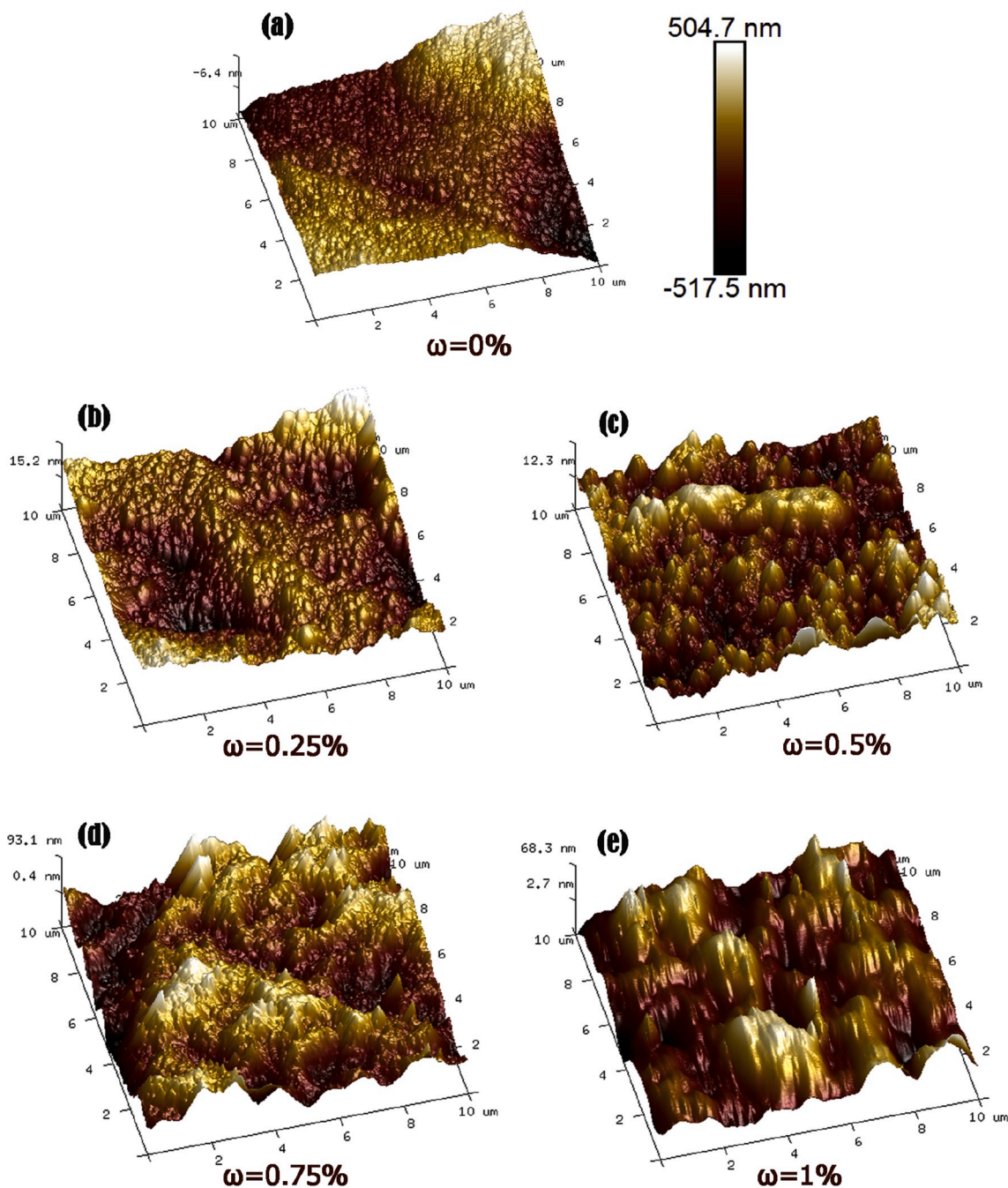| Fraction of $Sr_4Al_2O_4$: Eu^{2+}, Dy^{3+}(wt.%)	C (%)	Al (%)	Eu (%)
0	52.82	0	0
0.25	51.43	0.73	0.0073
0.50	52.39	0.58	0.0059
0.75	50.64	0.82	0.0083
1.00	51.70	1.73	0.0137

Fig. 5. SEM images of membrane top surfaces: (a)pristine PVDF membrane, (b) hybrid membrane with 0.25 wt% of nano-$Sr_4Al_2O_4$: Eu^{2+}, Dy^{3+}, (c) hybrid membrane with 0.50 wt% of nano-$Sr_4Al_2O_4$: Eu^{2+}, Dy^{3+}, (d) hybrid membrane with 0.75 wt% of nano-$Sr_4Al_2O_4$: Eu^{2+}, Dy^{3+}, (e) hybrid membrane with 1 wt% of nano-$Sr_4Al_2O_4$: Eu^{2+}, Dy^{3+}.

nanoparticles did not increase the luminescent intensity of the membranes, but slightly decreased this value as showed in Fig. 1 (c). The reason for this phenomenon is that the distribution of nano-$Sr_4Al_2O_4$: Eu^{2+}, Dy^{3+} as insoluble in the casting solution is affected by the viscosity of the casting solution. The slight decrease of the luminescent intensity of the hybrid membrane at the content of nanoparticles higher than 0.75 wt% may be due to the agglomeration/precipitation of the added nanoparticles at high content during the fabrication process of the hybrid membrane via NIPS, which would slightly weaken the luminescent capability of the hybrid membrane.

3.2. Contact angle measurement

In recent years, many researches showed that the hydrophilicity of the membrane had a pronounced influence on the anti-fouling performance of the membrane [23,24]. The measurement of the contact angle is an effective way to evaluate the hydrophilicity and wettability of the membrane surface [25,26]. Table 2 and Fig. 2 show the initial contact angle of different membranes and the change of contact angle with time. It was noticed that the contact angle of the pristine PVDF membrane was relatively high (89.9°), and gradually decreased with the addition of rare earth nanoparticles. When mass fraction of nano-$Sr_4Al_2O_4$: Eu^{2+}, Dy^{3+} reached up to 0.75 wt%, the contact angle decreased to 78.1 $\pm$ 4.70°. However, further increasing the mass fraction of nano-$Sr_4Al_2O_4$:
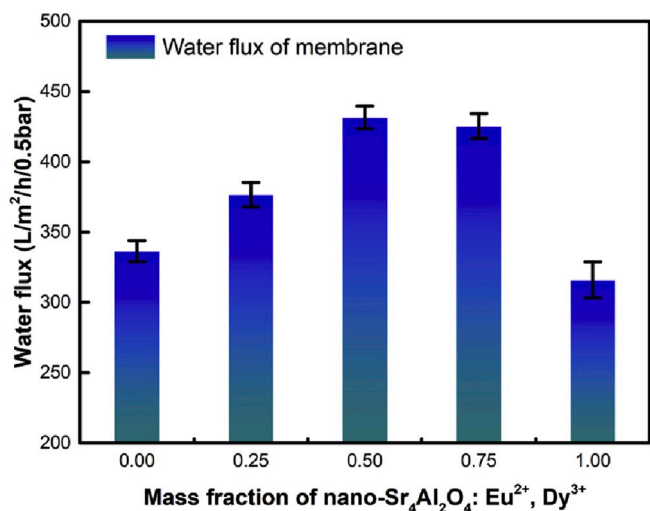
Fig. 6. Water flux of pristine PVDF and hybrid membrane.

Eu^{2+}, Dy^{3+} would not decrease the contact angle.

In addition, it should be pointed out that when the content of nano-$Sr_4Al_2O_4$: Eu^{2+}, Dy^{3+} was 0.75 wt%, it seemed to have a faster wetting rate than that of 1.00 wt%. These results confirm that the addition of rare earth nanoparticles can effectively improve the hydrophilicity of the membrane. Due to the large amount of metal hydrophilic particles in aluminate rare earth nanoparticles combined with traditional PVDF polymer materials, the membrane's hydrophilicity is effectively improved.

3.3. Membrane surface morphology

SEM images of the surface of the pristine PVDF membrane and hybrid membranes with different mass fraction of nano-$Sr_4Al_2O_4$: Eu^{2+}, Dy^{3+} are shown in Fig. 3. The statistics of pore size distribution are summarized in Table 3. The pristine PVDF membrane had an average pore size of 17 ± 4 nm, a pore density of 5.23×10^{13} m^{-2}, and a surface porosity of 3.78%. However, we could find that the pore density of the hybrid membranes decreased obviously with the increase of rare earth nanoparticles, while the pore size and surface porosity almost kept constant in the hybrid membranes except that the pore size of hybrid membrane with 0.50 wt% of nano-$Sr_4Al_2O_4$: Eu^{2+}, Dy^{3+} was obviously smaller (15 ± 3 nm). The cause of the decrease in the porosity of the membrane surface may be due to the addition of nano-$Sr_4Al_2O_4$: Eu^{2+}, Dy^{3+}, which causes a certain degree of blockage of the membrane pores.

As showed in Fig. 3(a–f) and Fig. S3, it could be found that nano-$Sr_4Al_2O_4$: Eu^{2+}, Dy^{3+} on membrane surface also increased with the content of these rare earth particles in the casting solution. EDX mapping images of hybrid membrane with 0.50 wt% of nano-$Sr_4Al_2O_4$: Eu^{2+}, Dy^{3+} confirmed the co-existence of Al and Eu elements on the surface of membrane, as showed in Fig. 3(g–i).

The precise contents of C, Al and Eu elements on different membrane surfaces are listed in Table 4. Compared with the pristine PVDF membrane, the C element on the hybrid membrane surface had no obvious change, but the Al element and Eu element on the membrane surface would gradually increase with the increase of rare earth nanoparticles.

3.4. Membrane cross section morphology

The process of membrane formation is essentially the result of the interaction among the solute (polymer), solvent and nonsolvent (water), which leads to phase separation [27–29]. In the casting phase, rare earth nanoparticles have great differences to PVDF in physical and chemical properties. Therefore, the doping of rare earth nanoparticles would inevitably cause changes in the internal thermodynamic stability and phase separation dynamics in the process of membrane formation, which would lead to changes in the structure, especially the cross-section structure of the membrane. Cross section SEM images of pristine PVDF membrane and hybrid membranes with different mass fraction of nano-$Sr_4Al_2O_4$: Eu^{2+}, Dy^{3+} are showed in Fig. 4. It can be found that the cross section of pristine PVDF membrane presented the arrangement structure of finger like pores, and the addition of a small amount of nano-$Sr_4Al_2O_4$: Eu^{2+}, Dy^{3+} (0.25 wt%) has no obvious effect on the membrane structure. But with the increase of the amount of nano-$Sr_4Al_2O_4$: Eu^{2+}, Dy^{3+} up to 0.75 wt%, the cross section structure of the membrane gradually changed from finger-like pores to sponge-like pores as showed in Fig. 4 (a), (b) and (c). On the wall of the pores, some rare earth particles and many small pores were evenly distributed on it, as showed in Fig. 4(e).

The content of C, Al and Eu elements on the local membrane section are analyzed by EDX, and the results are listed in Table 5. Compared with the data in Table 4, it could be found that the content of Al and Eu elements in the cross section was increased, indicating that the content of rare earth nanoparticles inside the hybrid membrane was higher than that on the surface. On the other hand, all these elements were evenly distributed in the cross-section structure, indicating that the distribution of rare earth nanoparticles inside the membrane was relatively uniform.

3.5. Membrane roughness

Fig. 5 shows the variation of membrane surface roughness by AFM

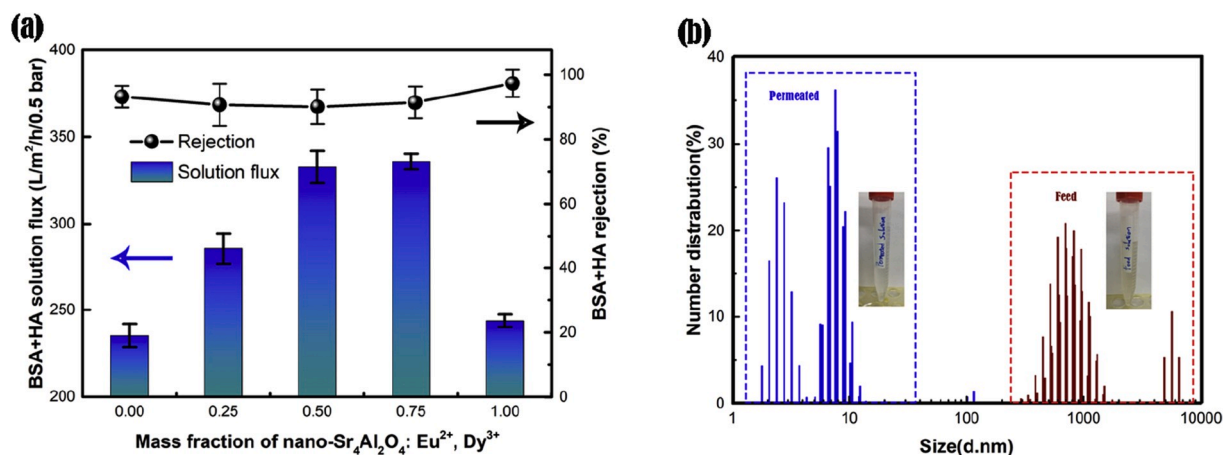**Fig. 7.** (a) BSA/HA aqueous solution flux and rejection rate of pristine PVDF and hybrid membrane with different content of nano-$Sr_4Al_2O_4$: Eu^{2+}, Dy^{3+}, (b) molecular size and distribution of the feed and the permeated solution treated from hybrid membrane with 0.75 wt% content of nano-$Sr_4Al_2O_4$: Eu^{2+}, Dy^{3+}.
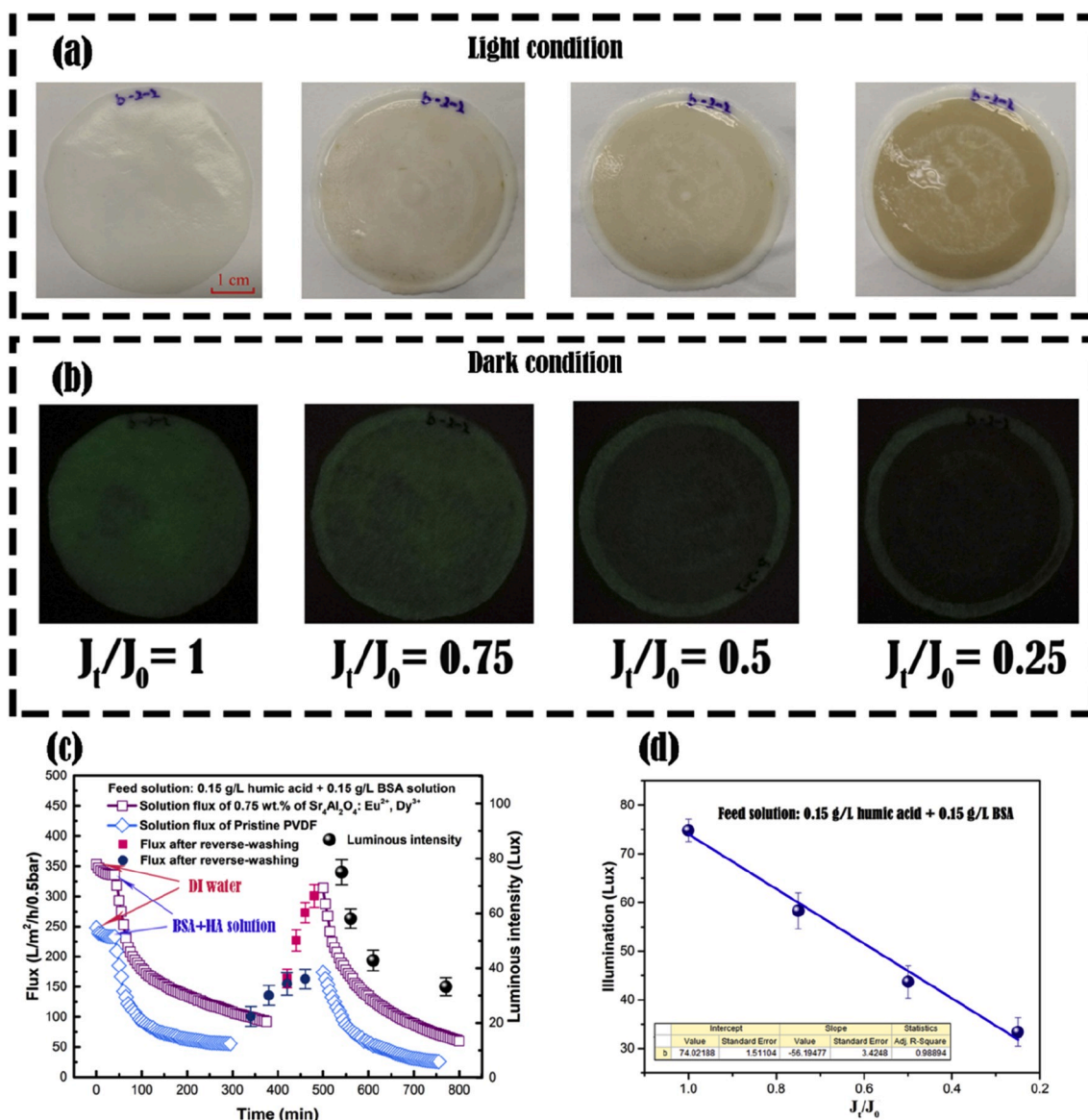
Fig. 8. The picture of hybrid membranes with 0.75 wt% of nano-Sr$_4$Al$_2$O$_4$: Eu^{2+}, Dy^{3+} at different pollution levels under light (a) and dark (b) conditions, (c) BSA/HA aqueous solution flux change of pristine PVDF membrane and hybrid membrane with 0.75 wt% of nano-Sr$_4$Al$_2$O$_4$: Eu^{2+}, Dy^{3+}, and its luminescent intensity change during permeability process, (d) The corresponding relationship between membrane's luminescent intensity and fouling degree for hybrid membrane with 0.75 wt% of nano-Sr$_4$Al$_2$O$_4$: Eu^{2+}, Dy^{3+}.
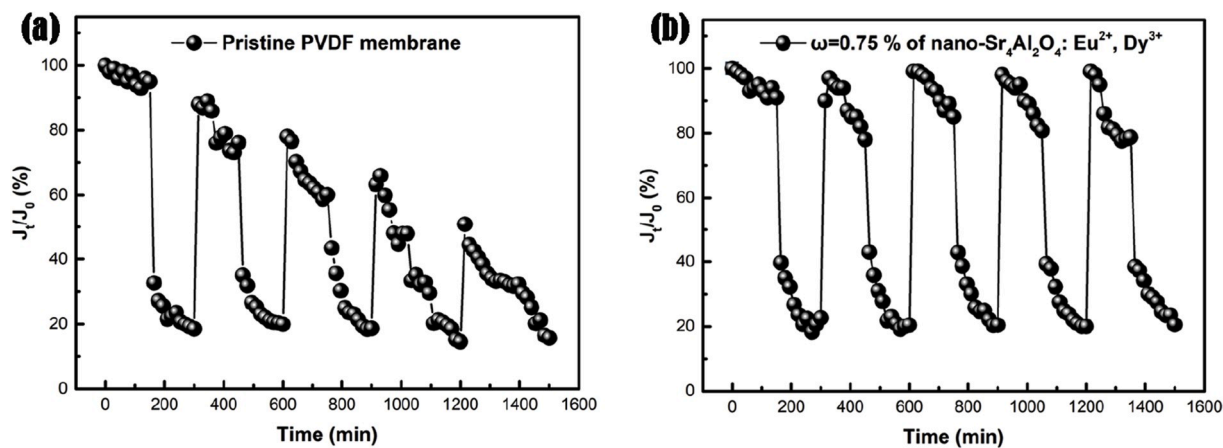

Fig. 9. BSA/HA aqueous solution flux attenuation rate of (a) pristine PVDF membrane and (b) hybrid membrane with 0.75 wt% of nano-Sr$_4$Al$_2$O$_4$: Eu^{2+}, Dy^{3+}.

analysis. The surface of the pristine PVDF membrane was relatively smooth, and a small amount of nano-$Sr_4Al_2O_4$: Eu^{2+}, Dy^{3+} (0.25 wt%) did not greatly affect on the surface roughness of the membrane as showed in Fig. 5(a) and (b). However, with the increase of nano-$Sr_4Al_2O_4$: Eu^{2+}, Dy^{3+} content, the surface roughness of the membrane increased. When the mass fraction of nano-$Sr_4Al_2O_4$: Eu^{2+}, Dy^{3+} reached 1.00 wt%, it seemed that some large bulges appeared on the surface of the membrane, which might be caused by the agglomeration of rare earth particles as showed in Fig. 5 (c), (d) and (e).

3.6. Membrane water flux

Deionized water does not contain impurities, when water passes through the membrane under pressure, membrane is not polluted, and could be repeatedly tested [30–32]. Therefore, the test of membrane water flux is an effective method to evaluate the membrane permeability [33,34]. The test of membrane water flux is determined by a professional membrane evaluation system platform named "Convergence Inspector", for which the specific information could be found in the supporting information, and the results are shown in Fig. 6. When the water pressure was set to 0.5 bar, the water flux of the pristine PVDF membrane was about 336.5 L/m^2/h. Along with the increase amount of nano-$Sr_4Al_2O_4$: Eu^{2+}, Dy^{3+}, the water flux of the hybrid membranes improved gradually. When the content of nano-$Sr_4Al_2O_4$: Eu^{2+}, Dy^{3+} was 0.50 wt%, the water flux of the hybrid membrane could reach its maximum of about 431.6 L/m^2/h, about 128.3% higher than the water flux of the pristine PVDF membrane. However, when further increasing nano-$Sr_4Al_2O_4$: Eu^{2+}, Dy^{3+} content to 1.00 wt%, the water flux decreased to about 316.1 L/m^2/h. The reason probably lies in that the addition of a small amount of nano-$Sr_4Al_2O_4$: Eu^{2+}, Dy^{3+} effectively improved the hydrophilicity and porosity of the membrane. Under the effect of the capillary effect, the water flux of the membrane had been effectively improved. However, due to the fact that rare earth nanoparticles are insoluble in water or organic solvents, too much nano-$Sr_4Al_2O_4$: Eu^{2+}, Dy^{3+} content would lead to the blocking of membrane pores, which eventually led to the decrease of membrane water flux. In addition, considering the small surface pore size of hybrid membrane with 0.50 wt% of nano-$Sr_4Al_2O_4$: Eu^{2+}, Dy^{3+} (15 ± 3 nm), which is also conducive to promoting the formation of capillary effects and increasing the water flux.

3.7. Membrane BSA/HA aqueous solution flux and rejection

In order to effectively simulate the operational situation of membrane treatment of sewage, the BSA/HA aqueous solution as the feed solution is used to carry out the filtration experiment, in which BSA is used as the macromolecular organic matter and humic acid as the micromolecular organic matter [35–37]. The permeability and rejection rate of membranes could be effectively evaluated by analyzing the initial flux of the feed solution and the rejection rate of pollutants. Fig. 7 (a) demonstrates the BSA/HA aqueous solution flux and rejection rate of pristine PVDF and hybrid membrane with different content of nano-$Sr_4Al_2O_4$: Eu^{2+}, Dy^{3+}. The flux of the feed solution increased along with the content of nano-$Sr_4Al_2O_4$: Eu^{2+}, Dy^{3+}, similar to the result of membrane water flux. When the content of nano-$Sr_4Al_2O_4$: Eu^{2+}, Dy^{3+} reached 0.50 wt%, the maximum aqueous solution flux of the hybrid membrane was 335.8 L/m^2/h, 142% higher than that of the original PVDF membrane (235.2 L/m^2/h). Besides, the rejection rate of BSA/HA aqueous solution by different membranes was analyzed. Although in a certain range, with the increase of the amount of nano-$Sr_4Al_2O_4$: Eu^{2+}, Dy^{3+}, the rejection rate of the membrane slightly decreased from 93.2% for pristine PVDF membrane to 90.7% for hybrid membrane with 0.75 wt% of nano-$Sr_4Al_2O_4$: Eu^{2+}, Dy^{3+}, but the rejection rate of all organic solute could be maintained at a high level. Too many nano-$Sr_4Al_2O_4$: Eu^{2+}, Dy^{3+} would lead to a sharp decrease in the flux of aqueous solution, but the rejection rate of the membrane increased to 97.3%.

In addition, the particle size and distribution before and after filtration by hybrid membrane with 0.75 wt% content of nano-$Sr_4Al_2O_4$: Eu^{2+}, Dy^{3+} were analyzed by dynamic light scattering (DLS), and the result was shown in Fig. 7 (b). It can be found by naked eyes that the feed solution is yellowish due to the existence of humic acid, while the permeate solution is colorless and transparent, indicating the effective filtration of pollutants. Meanwhile, the results also showed that the molecular size of solute in feed solution was about 1,000 nm and 10,000 nm, and the size of permeated solution was below 10 nm, confirmed that all these membranes demonstrated an effective filtration performance.

3.8. Real time characterization of the fouling degree of membranes

The doping of rare earth nanoparticles endows the hybrid membrane with self-luminescent performance, thus the real time characterization of membrane's fouling can be realized by these hybrid membranes. Fig. 8(a) and (b) shows the images taken at different fouling degree under illustration and dark conditions. We can see that the center area of the membrane is getting yellower as the fouling degree increases through the whole filtration time under the illumination condition; while the center area looks darker with the increasing degree of fouling under the dark condition. The illumination at the center area decreases linearly with the fouling degree, with the slope of −56.19 and the correlation coefficient of 0.99, as shown in Fig. 8 (d). This linear relationship demonstrated that the luminescent intensity of the hybrid membrane could be a facile, direct and effective indicator to precisely evaluate its fouling degree.

Notably, the illumination intensity of the hybrid membrane increases with the back washing time, as shown in Fig. 8 (c). It means that the illumination of the hybrid membrane restores as the recovery of its permeability, proving that the hybrid nanoparticles can be validly and effectively used as the indicator for the degree of fouling of membranes at the back washing process. Thus, it can conveniently display the fouling degree of membranes, real time showing its fouling/cleaning degree during the whole operation period, benefiting optimizing the filtration/back washing process and further improving the separation efficiency of the membrane.

Meanwhile, the flux of the mimic sewage of the hybrid membrane is at least 20% (50 L/m^2/h) higher than that of pristine counterpart during the whole operation period, showing better permeability of the hybrid membrane, as shown in Fig. 8 (c). The flux of the hybrid membrane drops to 20% of its original value after nearly 380 min, instead of 300 min for its pristine counterpart, displaying a decreased flux attenuation rate and an improved anti-fouling property of the hybrid membrane during filtration.

3.9. Membrane anti-fouling performance

In order to further characterize the effect of hybrid rare earth nanoparticles on the anti-fouling performance of the membrane, the pollution and backwash experiments are repeatedly carried out on membranes, and the results are showed in Fig. 9. The BSA/HA aqueous solution flux of the original PVDF membrane was only about 50% of the initial after 4 pollution-backwash cycles. On the contrary, for the hybrid membrane with 0.75 wt% of nano-$Sr_4Al_2O_4$: Eu^{2+}, Dy^{3+}, the flux was still more than 95% of the initial value under the same experimental process. This result means that adding rare earth nanoparticles in the membrane clearly improved the anti-fouling properties of the membrane.

4. Conclusion

In this paper, we reported a robust and simple approach to synthesize a self-luminescent membrane, which mainly composed of polymer and rare earth up conversion luminescent nanoparticles. This self-luminescent membrane can be used as indicator to real-time

characterize the fouling/cleaning degree of itself. Moreover, the anti-fouling property was improved due to the hybrid of these hydrophilic rare-earth nanoparticles in the membrane. With the increase of the content of this nano-$Sr_4Al_2O_4$: Eu^{2+}, Dy^{3+}, the water flux of the hybrid membranes rose first and then declined, with the rejection rate at a high level. The contact angle of membranes showed that the hydrophilicity of the membrane was also improved by these inorganic components. SEM and AFM confirmed the uniform distribution of these nanoparitcle, which increased the irregularity degree of hybrid membrane surface. This self-luminescent membrane may open a new way to many potential applications, including real time indicator for the fouling/cleaning degree, intelligent recognition and detection etc.

Declaration of competing interest

The authors declare that they have no conflict of interest.

Acknowledgement

Appendix A. Supplementary data

Supplementary data to this article can be found online at https://doi.org/10.1016/j.memsci.2020.118123.

References

[1] C. Zhao, S. Nie, T. Min, S. Sun, Polymeric pH-sensitive membranes - a review, Prog. Polym. Sci. 36 (2011) 1499–1520.

[2] F. Kai, J. Huang, H. Yang, R. Lu, X. Sun, Z. Hou, pH and thermal-dependent ultra filtration membranes prepared from poly (methacrylic acid) grafted onto polyethersulfone synthesized by simultaneous irradiation in homogenous phase, J. Membr. Sci. 543 (2017) 335–341.

[3] J. Shaoyi, C. Zhiqiang, Ultralow-fouling, functionalizable, and hydrolyzable zwitterionic materials and their derivatives for biological applications, Adv. Mater. 22 (2010) 920–932.

[4] J. Wang, Z. Han, X. Yang, J. Shuang, W. Lv, Z. Jiang, Z.Q. Shi, Enhanced water retention by using polymeric microcapsules to confer high proton conductivity on membranes at low humidity, Adv. Funct. Mater. 21 (2015) 971–978.

[5] X. Rui, C. Liang-Yin, D. Jin-Gen, Membranes and membrane processes for chiral resolution, ChemInform 37 (2008) 1243–1263.

[6] C.C. Ho, A.L. Zydney, Transmembrane pressure profiles during constant flux. Microfiltration of bovine serum albumin, J. Membr. Sci. 209 (2002) 363–377.

[7] G. Sun, C. Zhang, W. Li, L. Yuan, S. He, L. Wang, Effect of chemical dose on phosphorus removal and membrane fouling control in a UCT-MBR, Front. Environ. Sci. Eng. 13 (2018) 136–149.

[8] B. Hu, X. Zuo, J. Xiong, H. Yang, M. Cao, S. Yu, Identification of fouling mechanisms in MBRs at constant flowrate: model applications and SEM-EDX characterizations, Water Sci. Technol. 77 (2018) 229–238.

[9] C.C. Boyd, S.J. Duranceau, Evaluation of ultrafiltration process fouling using a novel transmembrane pressure (TMP) balance approach, J. Membr. Sci. 446 (2013) 456–464.

[10] C. Minhua, W. Xinglong, H. Xiaoyan, H. Changwen, Microemulsion-mediated solvothermal synthesis of $SrCO_3$ nanostructures, Langmuir 21 (2005) 6093–6102.

[11] I.Z. Dinic, M.E. Rabanal, K. Yamamoto, Z. Tan, O.B. Milosevic, PEG and PVP assisted solvothermal synthesis of $NaYF_4$: Yb^{3+}/Er^{3+} up-conversion nanoparticles, Adv. Powder Technol. 27 (2015) 845–853.

[12] S.E. Kichanov, D.P. Kozlenko, Y.E. Gorshkova, G.E. Rachkovskaya, B.N. Savenko, Structural studies of nanoparticles doped with rare-earth ions in oxyfluoride lead-silicate glasses, J. Nano Res. 20 (2018) 54–76.

[13] L. Tsonev, Luminescent activation of planar optical waveguides in $LiNbO_3$ with rare earth ions Ln^{3+} – a review, Opt. Mater. 30 (2008) 892–899.

[14] N. Maximous, G. Nakhla, W. Wan, K. Wong, Preparation, characterization and performance of Al_2O_3/PES membrane for waste water filtration, J. Membr. Sci. 341 (2009) 67–75.

[15] Y. Lu, Y.S. Li, C.B. Xiang, S. Xianda, Effect of nano-sized Al_2O_3-particle addition on PVDF ultrafiltration membrane performance, J. Membr. Sci. 276 (2006) 162–167.

[16] Y. Lu, Y.S. Li, C.B. Xiang, Preparation of poly(vinylidene fluoride)(pvdf) ultrafiltration membrane modified by nano-sized alumina (Al_2O_3) and its antifouling research, Polymer 46 (2005) 7701–7706.

[17] J.F. Li, Z.L. Xu, H. Yang, L.Y. Yu, M. Liu, Effect of TiO_2 nanoparticles on the surface morphology and performance of microporous PES membrane, Appl. Surf. Sci. 255 (2009) 4725–4732.

[18] Y. Yang, H. Wang, J. Li, B. He, S. Liao, Novel functionalized nano-TiO_2 loading electrocatalytic membrane for oily wastewater treatment, Environ. Sci. Technol. 46 (2012) 6815–6821.

[19] R.K. Manoharan, S. Ayyaru, Y.H. Ahn, Auto-cleaning functionalization of the polyvinylidene fluoride membrane by the biocidal oxine/TiO_2 nanocomposite for anti-biofouling properties, New J. Chem. 44 (2020) 807–816.

[20] F. Parvizian, S.M. Hosseini, A.R. Hamidi, S.S. Madaeni, A.R. Moghadassi, Electrochemical characterization of mixed matrix nanocomposite ion exchange membrane modified by ZnO nanoparticles at different electrolyte conditions "pH/concentration", J. Taiwan. Inst. Chem. E. 45 (2014) 2878–2887.

[21] M. Nermen, N. George, W. Wan, K. Wong, Performance of a novel ZrO_2/PES membrane for wastewater filtration, J. Membr. Sci. 352 (2010) 222–230.

[22] R.Z. Pang, X. Li, J.S. Li, Z.Y. Lu, C. Huang, X.Y. Sun, L.J. Wang, In situ preparation and antifouling performance of $ZrO_2/PVDF$ hybrid membrane, Acta Phys. Chim. Sin. 29 (2013) 2592–2598, 2597.

[23] N.A. Alenazi, M.A. Hussein, K.A. Alamry, A.M. Asiri, Modified polyether-sulfone membrane: a mini review, Des. Monomers Polym. 20 (2017) 532–546.

[24] B.S. Lalia, V. Kochkodan, R. Hashaikeh, N. Hilal, A review on membrane fabrication: structure, properties and performance relationship, Desalination 326 (2013) 77–95.

[25] R. Kumar, A.F. Ismail, Fouling control on microfiltration/ultrafiltration membranes: effects of morphology, hydrophilicity, and charge, J. Appl. Polym. Sci. 132 (2015) 235–252.

[26] M.S. Sri Abirami Saraswathi, A. Nagendran, D. Rana, Tailored polymer nanocomposite membranes based on carbon, metal oxide and silicon nanomaterials: a review, J. Mater. Chem. A. 7 (2019) 8723–8745.

[27] J. Kim, J. Kim, Y.M. Lee, E. Drioli, Thermally-induced phase separation (TIPS) and electrospinning methods for emerging membrane applications: a review, AIChE J 62 (2015) 265–284.

[28] P.V.D. Witte, P.J. Dijkstra, J.W. Berg, J. Feijen, Phase separation processes in polymer solutions in relation to membrane formation 117 (1996) 1–31.

[29] G. Guillen, Y. Pan, M. Li, E. Hoek, Preparation and characterization of membranes formed by nonsolvent induced phase separation: a review, Ind. Eng. Chem. Res. 50 (2011) 147–176.

[30] N. Zhang, W. Qi, L. Huang, E. Jiang, B. Junjiang, X. Zhang, B. An, G. He, Review on structural control and modification of graphene oxide-based membranes in water treatment: from separation performance to robust operation, Chin. J. Chem. Eng. (2019) 27–44.

[31] N. Song, X. Gao, Z. Ma, X. Wang, Y. Wei, C. Gao, A review of graphene-based separation membrane: materials, characteristics, preparation and applications, Desalination 437 (2018) 59–72.

[32] S. Habibi, A. Nematollahzadeh, Enhanced water flux through ultrafiltration polysulfone membrane via addition-removal of silica nano-particles: synthesis and characterization, J. Appl. Polym. Sci. 133 (2016) 219–231.

[33] S. Zhao, L. Zou, C. Tang, D. Mulcahy, Recent developments in forward osmosis: opportunities and challenges, J. Membr. Sci. 396 (2012) 1–21.

[34] J. Wang, Z. Wang, S. Wang, Improving the water flux and bio-fouling resistance of reverse osmosis (RO) membrane through surface modification by zwitterionic polymer, J. Membr. Sci. 493 (2015) 188–199.

[35] N. Shoparwe, T. Otitoju, A.L. Ahmad, Fouling evaluation of polyethersulfone (PES)/sulfonated cation exchange resin (SCER) membrane for BSA separation, J. Appl. Polym. Sci. (2017) 45–54.

[36] H. Mo, K. Tay, H. Ng, Fouling of reverse osmosis membrane by protein (BSA): effects of pH, calcium, magnesium, ionic strength and temperature, J. Membr. Sci. 315 (2008) 28–35.

[37] C. Chen, L. Tang, B. Liu, X. Zhang, J. Crittenden, K.L. Chen, Y. Chen, Forming mechanism study of unique pillar-like and defect-free PVDF ultrafiltration membranes with high flux, J. Membr. Sci. 487 (2015) 1–11.